



Cite this: DOI: 10.1039/d1ee03961j

A highly efficient constant-voltage triboelectric nanogenerator†

Xinyuan Li, ^{‡a} Chuguo Zhang, ^{‡ab} Yikui Gao, ^{‡ac} Zhihao Zhao, ^a
Yuxiao Hu, ^{ac} Ou Yang,^{ab} Lu Liu, ^{ab} Linglin Zhou, ^{ab} Jie Wang ^{*abc} and
Zhong Lin Wang ^{*abcd}

The rapid development of the Internet of Things and artificial intelligence has led to an increase in attention focused on distributed power sources such as triboelectric nanogenerators (TENGs), however, enhancing the energy output from TENGs is crucial for their large-scale application. Here, a constant-voltage TENG (CV-TENG) based on a phase-shift design is presented to enhance the energy output *via* converting a conventional pulse-voltage output into a constant-voltage one and decreasing the crest factor to 1.03. The average power is unexpectedly increased 1.9-fold compared with that of a pulse-voltage TENG (PV-TENG) without a phase-shift design. The energy enhancement is even more than 3-fold under a capacitance load in response to a low-frequency input. Furthermore, the dynamic process of charge transfer under a capacitance load is revealed, which gives a theoretical guide to improving the energy-output efficiency of a TENG toward 100%. This work provides a paradigm shift when it comes to achieving high-efficiency CV-TENGs, and it is of great importance for the acceptance of TENGs as a major form of energy technology.

Received 28th December 2021,
Accepted 7th February 2022

DOI: 10.1039/d1ee03961j

rsc.li/ees

Broader context

With the development of the Internet of Things and artificial intelligence, billions of moving objects around the world can be interconnected *via* wireless signals, and each needs to be powered. A possible strategy is to make each device self-powered *via* employing triboelectric nanogenerators (TENGs) to harvest energy from the surrounding environment. As a distributed power source, a TENG acts as a promising candidate for integration with multifunctional electronics due to its low cost, light weight, and high efficiency at low frequencies. However, there are several key issues hampering the application of TENGs: the inherent high crest factor output of TENGs is not suitable for existing electronics, the low average power and energy-output inefficiencies relating to pulse-voltage TENGs (PV-TENGs) limit their application, and direct contact between the electrode and dielectric layer usually results in a short working lifetime. These nonnegligible issues limit the development of TENGs into a major form of energy technology. In this work, a universal and practical method is proposed to convert a conventional pulse-voltage approach into a constant-voltage, using a phase-shift design. Combining this with a unique adaptive contact structure, several key issues mentioned above could be addressed simultaneously in our work. The constant-voltage TENG (CV-TENG) exhibits excellent integrated electrical performance that exceeds that of a conventional PV-TENG, representing great progress in the field of TENG-based distributed power sources.

Introduction

The rapid development of the Internet of Things (IoTs), artificial intelligence (AI), and implantable medical devices has created huge demand for ubiquitous, portable, and distributed power sources.^{1,2} Triboelectric nanogenerators (TENGs) are a desirable choice due to their ability to convert mechanical energy from the environment into electrical energy effectively.^{3–6} Recently, TENGs have remained an active choice for supporting fast developments in the areas of the IoTs, AI, energy science, self-powered sensors, environmental protection, medical science, wearable electronics, and robotics as TENGs are a core component of potential technologies with great prospective applications.^{7–10}

^a CAS Center for Excellence in Nanoscience, Beijing Key Laboratory of Micro–Nano Energy and Sensor, Beijing Institute of Nanoenergy and Nanosystems, Chinese Academy of Sciences, Beijing 100083, P. R. China. E-mail: wangjie@bin.cas.cn

^b School of Nanoscience and Technology, University of Chinese Academy of Sciences, Beijing 100049, P. R. China

^c Center on Nanoenergy Research, School of Physical Science and Technology, Guangxi University, Nanning, 530004, P. R. China

^d School of Materials Science and Engineering, Georgia Institute of Technology, Atlanta, GA 30332-0245, USA. E-mail: zhong.wang@mse.gatech.edu

† Electronic supplementary information (ESI) available. See DOI: 10.1039/d1ee03961j

‡ These authors contributed equally to this work.

As a distributed power source or core component in self-powered systems, it is essential that TENGs exhibit excellent output performance.^{11,12} Based on a coupling effect involving contact electrification and electrostatic induction, TENGs exhibit a pulse-voltage and high crest factor under a resistance load, limiting their ability to act as a distributed power source to drive small electronics directly^{13,14} (here the crest factor is the ratio between the peak current and equivalent current). Although such problems could be solved by connecting a rectifier and energy storage unit, the energy-output efficiency of direct charging is very low due to the unmatched resistance.¹⁵ In spite of a lot of research having been devoted to promoting energy-transfer efficiency and energy-storage efficiency based on power management, the maximum energy-output efficiency of a pulse-voltage TENG (PV-TENG) is only 50% when evaluated using a V-Q plot, which exposes the inherent weaknesses of PV-TENGs in terms of energy output.^{5,15-18} Moreover, the high crest factor of PV-TENGs leads to low average power outputs, far from the peak power, seriously hindering their application in the areas of artificial intelligence and the Internet of Things as distributed power sources.^{14,18}

As a distributed power source, improving the average power of a TENG, which is thought to be related to the surface charge density, is a crucial problem preventing its commercial application. Therefore, large amounts of effort have been devoted to improving the amount of charge density by means of material improvement, structural optimization, surface modification, and so on to boost the energy output,¹⁹⁻²¹ with little attention being paid to the TENG voltage. In other power sources, such as solar cells, pyroelectrics, piezoelectric generators, and energy storage devices, voltage always plays an indispensable role when it comes to energy output and charge transfer.²²⁻²⁴ However, it is unclear whether the voltage of a TENG has important effects on the energy output and charge transfer. Gaining a fundamental understanding of energy output and charge transfer is of great importance for the development of TENGs into a major form of energy technology. Therefore, a thorough and comprehensive study is required to gain insight into energy output and charge transfer in terms of the TENG voltage under common loads.

In this work, a constant-voltage TENG (CV-TENG) is realized *via* a phase-shift design from a conventional PV-TENG, producing a significantly higher energy output than a PV-TENG that can power electronics directly. It can significantly decrease the crest factor to 1.03, nearly obtaining direct current (crest factor = 1). The average power is unexpectedly increased 1.9-fold compared with a conventional PV-TENG without a phase-shift design, and the energy enhancement is over 3-fold under a capacitance load at low frequency; these results show that the phase-shift design is a universal and practical approach for promoting the energy output from TENGs effectively. Meanwhile, this work reveals the dynamic process of charge transfer under a capacitance load, which gives a theoretical guide to improving the energy-output efficiency from a TENG toward 100%. Furthermore, the lifetime of the CV-TENG is also tremendously extended through using an adaptive contact design between the electrode and dielectric material.

This work provides key parameters for obtaining TENGs with maximum average power and it presents a paradigm shift for achieving highly efficient CV-TENGs, which is of great importance for improving TENGs into a major form of energy technology.

Results and discussion

The structure and working mechanism of the CV-TENG

The structure of the CV-TENG with a rational phase-shift design is presented in Fig. 1a-c, and it consists of two main parts: a rotor and a stator. The rotor is a disc with six radial but irregularly arrayed trenches, employing the strategy of a phase-shift design,^{25,26} where dielectric layers are inserted in the trenches (Fig. 1a and Fig. S1 ESI†). The stator is another disc with twelve radial and regularly arrayed electrode sectors. The rotor and stator are stacked in the vertical direction in coaxial alignment (Fig. 1b), where the gap distance is about 1.0 cm. The positions of the dielectric layer are exhibited in Fig. 1c and Fig. S1 (ESI†). Different from the use of the same angles between trenches with fixed dielectric layers in a conventional PV-TENG, the phase-shift design selects the most qualified angle based on a strategy of reducing the crest factor effectively.^{25,26} The optimization of the phase-shift design is determined based on the number of individual TENG units, and the six single TENG units in our designed TENG correspond to a staggered 1/6 phase, which is the most effective way to reduce the crest factor of the current output. Therefore, the phase-shift design converts a single phase to six different phases with an equal phase shift on the rotor compared with a conventional PV-TENG. Details of the circuit connections between electrodes are exhibited in Fig. S2 (ESI†); each pair of adjacent electrodes on the stator serves as the two electrodes of a single TENG unit and are connected in parallel after connecting a full-wave rectifier. The operation of the CV-TENG relies on relative rotation between the rotor and stator, in which unique coupling between contact electrification and electrostatic induction gives rise to alternating flows of electrons between the electrodes. The current and voltage outputs of every single TENG unit in the CV-TENG exhibit the same shape but different phases, which is the essential difference from a PV-TENG (Fig. 1d, e and Fig. S3, S4 ESI†). Therefore, the superposition of the six current/voltage phases results in a constant-current/voltage output based on Kirchhoff's law and the linear circuit superposition principle. The continuous constant-current output of the CV-TENG also increases from 0.02 to 0.26 mA as the rotating frequency gradually increases, while the constant-voltage output is always stabilized at ~1400 V (Fig. 1f and g). The internal impedance of the TENG decreases upon an increase in the frequency, enhancing the current, and the peak voltage of the TENG does not vary with frequency, which is consistent with previous reports.²⁰

Generally, the typical crest factor of a conventional PV-TENG without a phase-shift design is as high as 6-12,^{13,19} which may seriously influence the working lifetime and capacity performance in terms of driving electronics directly or charging an energy

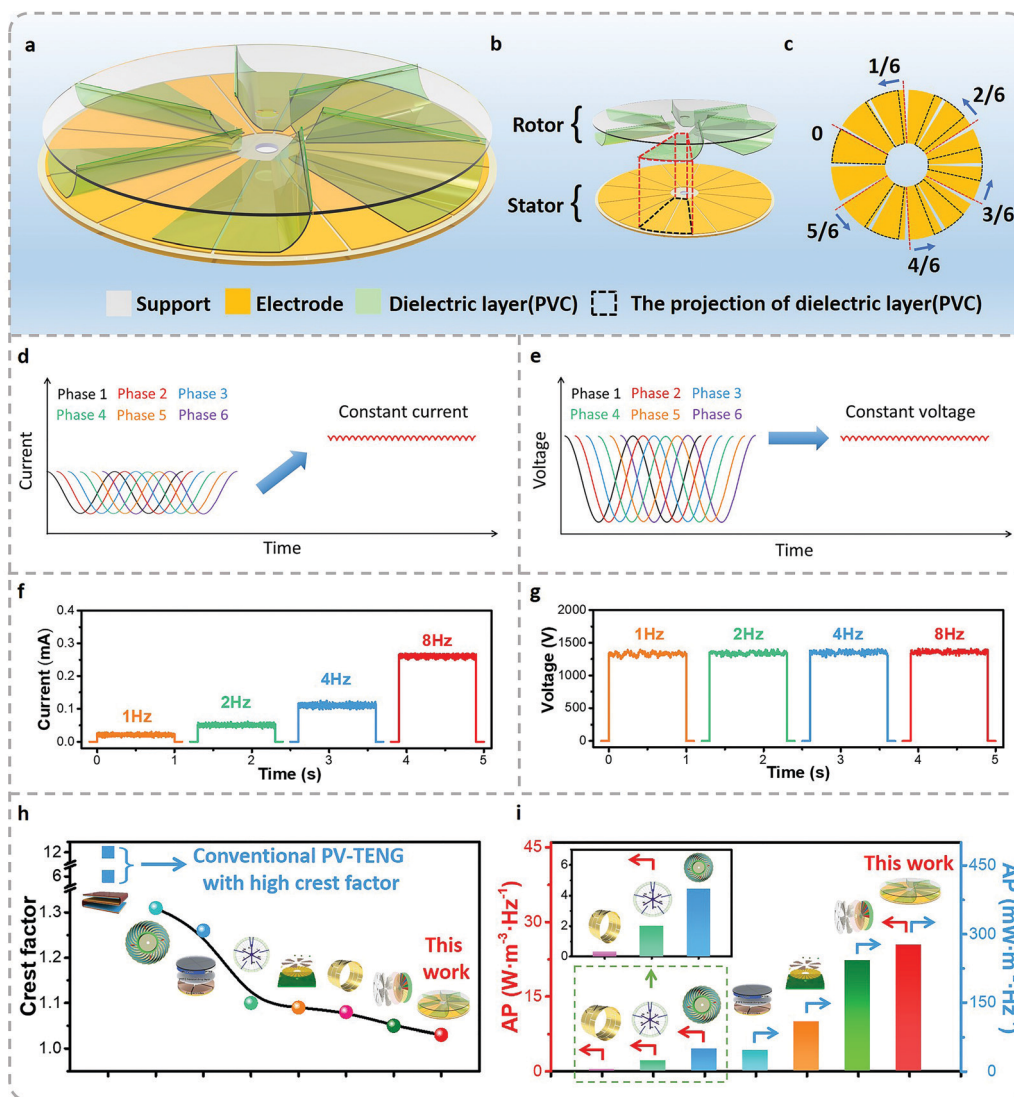


Fig. 1 The structure and working mechanism of the CV-TENG. (a) A schematic illustration of the CV-TENG. (b) The composition of the CV-TENG with two parts: a rotor and a stator. (c) A detailed view of the projection of the dielectric layer. Schematic diagrams of the superposition of (d) current and (e) voltage based on the phase-shift design. The (f) current and (g) voltage of the CV-TENG at different frequencies. A comparison of the (h) crest factor and (i) average power (AP) of the CV-TENG with other TENGs.

storage unit. The peak current and average current of the CV-TENG show only a slight difference, and the crest factor decreases to a value as low as 1.03 (Fig. S5 ESI†). This means that the phase-shift design is an effective way to decrease the crest factor and obtain a constant-current/voltage output. Due to the extensive efforts of researchers in recent years, the crest factor could be gradually decreased from 6–12 to 1.03 based on an accurate phase-shift design, and the average power was successfully improved from $0.29 \text{ W m}^{-3} \text{ Hz}^{-1}$ to $25.4 \text{ W m}^{-3} \text{ Hz}^{-1}$ based on structure design and material selection, as shown in Fig. 1h, i and Fig. S6, Table S1 (ESI†).^{19,26–30} Detailed discussion is provided in Note S1 (ESI†).

The output performance of the CV-TENG under a resistance load

Even though the high voltage ($\sim \text{kV}$) and low current ($\sim \mu\text{A}$) characteristics of TENGs does not suit existing electronics, they

work well with the help of power management systems.^{5,18,31} Therefore, exploring the maximum average power output of a TENG is of great significance when judging whether it has the ability to supply high effective power continuously, which is of great importance for the development of TENGs into a major form of energy technology. The output performances of the CV-TENG and PV-TENG under a resistance load are shown in Fig. 2. The current output shape from the CV-TENG under different resistance loads is always close to direct current with a low crest factor, while the output from the PV-TENG is in the form of a pulse signal under similar loads, as shown in Fig. 2a and b. The voltage output shapes from the CV-TENG and PV-TENG under different resistance loads are also consistent with this tendency, as shown in Fig. S7 and S8 (ESI†).

Furthermore, the differences between the peak current and valley current for the CV-TENG and PV-TENG under different

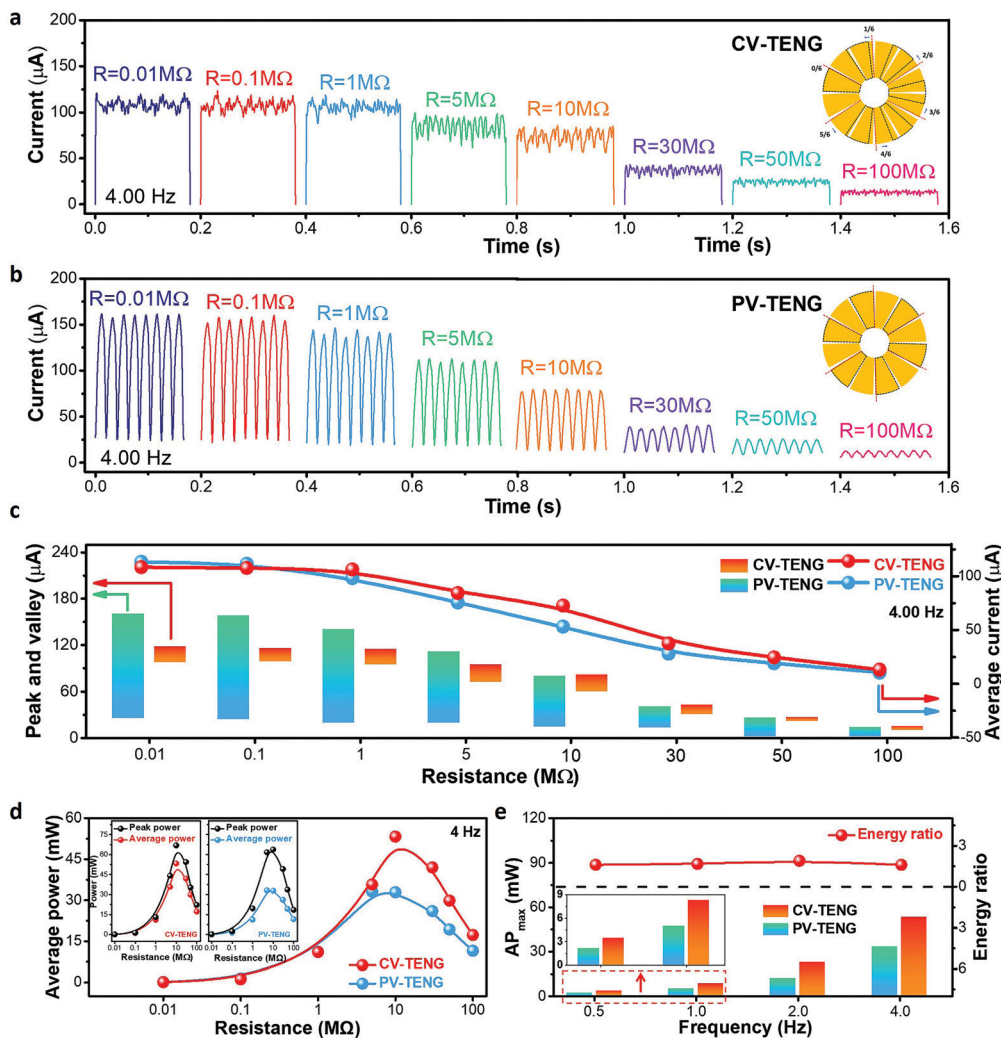


Fig. 2 The output performance of the CV-TENG under a resistance load. The current outputs of (a) a CV-TENG and (b) a PV-TENG under different resistance loads. (c) The peak currents, valley currents, and average currents of a CV-TENG and PV-TENG under different resistance loads. (d) A comparison of the average power between a CV-TENG and PV-TENG over a resistance load range from 0.01 to 100 M Ω ; inset: a comparison of the average power and peak power between a CV-TENG (left) and PV-TENG (right) under resistance loads. (e) The maximum average power (AP) of a CV-TENG and PV-TENG and their energy ratios at different frequencies.

resistance loads are presented in Fig. 2c and Fig. S3, Table S2 (ESI †). The conventional PV-TENG has inherent pulsed current, which leads to a large difference between the peak and valley current. The CV-TENG overcomes this issue with the help of the phase-shift design, acquiring a continuous direct-current output with a low crest factor, even in response to different resistance loads. As the resistance load is continually increased, it begins to limit the charge flow rate, making the average current decrease, as shown in Fig. 2c. The induced voltage will hold for a long time due to the screening effect,³² which leads to the peak voltage of the PV-TENG gradually getting close to the voltage of the CV-TENG with an increase in the resistance load (Fig. S7 and S8 ESI †). Here, the differences between the CV-TENG and PV-TENG are not only presented in terms of the shape of the voltage and current outputs, but they are also reflected in the electric quantity and energy output. The CV-TENG has the ability to generate a higher electric quantity

and energy output than the PV-TENG due to the presence of a constant induced voltage.³²

Generally, average current (I_{AC}) is a common and fair metric used to define the electric quantity obtained from a distributed power source. As shown in Fig. 2c, there is no significant difference between the PV-TENG and CV-TENG, with average current values of 0.11 mA and 0.10 mA, respectively, under a low resistance load of 0.01 M Ω . This changes as the resistance load increases, e.g., the CV-TENG exhibits a higher average current of 0.07 mA than the PV-TENG (0.05 mA), with an approximately 1.4-fold increase under a resistance load of 10 M Ω .

Besides a comparison of electric quantity, it is essential to evaluate the energy output of a TENG as a distributed power source; average power is an effective and equitable metric for evaluating the energy outputs of CV-TENGs and PV-TENGs. The average power under a resistance load (P_A^{PR}) can be calculated

via the following equation:

$$P_{AP}^R = \frac{\int_t^{t+\Delta T} I^2 R dt}{\Delta T} \quad (1)$$

where I is the experimental current, R represents the resistance load, and ΔT is the measured time. As shown in Fig. 2d, the CV-TENG can obtain a maximum average power of 53.29 mW under a resistance load of 10 M Ω , which is a 61.9% increase compared with the PV-TENG (maximum average power of 32.91 mW). Although PV-TENGs have attracted much attention due to their high peak power density,¹⁸ it is still difficult to achieve a high average power with the same value as the peak power output. Compared with the PV-TENG, the CV-TENG shows a greatly reduced difference between the average power and peak power, as shown in the inset of Fig. 2d, which points to an effective approach for moving the average power close to the peak power during TENG operation.

In addition, a comparison of the maximum average power between the CV-TENG and PV-TENG at different frequencies is exhibited in Fig. 2e and Fig. S9 (ESI[†]). The PV-TENG can obtain maximum average power values of 2.15, 4.98, 11.94, and 33.20 mW at 0.5, 1, 2, and 4 Hz, respectively, while the CV-TENG can obtain higher maximum average power values of 3.47, 8.33, 22.71, and 53.29 mW, respectively. In a word, the CV-TENG always shows great superiority in terms of the power output performance under a resistance load (1.6–1.9-fold increase) compared with the PV-TENG at different frequencies, which means that the phase-shift design is a practical approach for significantly improving the energy output.

The output performance of the CV-TENG under a capacitance load

Excellent TENG output performance is essential if a TENG is to act as a distributed power source or key component in self-powered systems.^{32–35} Considering that existing mature power management systems all need a capacitor to acquire electrical energy from the TENG first, it is worth deeply investigating the performances of CV-TENGs and PV-TENGs under a capacitance load with the aim of acquiring maximum average power.^{5,17,18,31}

Here the performances of CV-TENGs and PV-TENGs under a capacitance load are evaluated using a single capacitor (0.22 μ F), where the CV-TENG and PV-TENG are controlled by switches K_1 and K_2 , respectively, when connecting to the capacitor (Fig. 3a). Fig. 3b–e presents the voltage of the capacitor, the energy stored in the capacitor, the amount of charge flowing to the capacitor per cycle and the energy flowing to the capacitor per cycle as a function of the cycle number when charging with a CV-TENG and PV-TENG under the same mechanical motion with a frequency of 1 Hz. Detailed information is given in Note S2 (ESI[†]). The voltages of the capacitor charged by the CV-TENG and PV-TENG gradually increase to 989.47 V and 639.92 V, respectively, signifying that the CV-TENG has a higher charging rate than the PV-TENG over the same number of charging cycles (Fig. 3b). Meanwhile, the energy output from the CV-TENG shows a gradual increase to 2.4 times that from the PV-TENG as the number of cycles

increases; the CV-TENG only takes 25 cycles to store 107.69 mJ, far more than the PV-TENG (45.04 mJ) (Fig. 3c and Fig. S10 ESI[†]).

In addition, the charge flowing to the capacitor per cycle is a key parameter for evaluating the electric quantity output abilities of a TENG under a capacitance load, similar to how average current can be used to standardize the electric quantity output of a TENG under a resistance load. As shown in Fig. 3d, the CV-TENG exhibits excellent superiority in transferring charge to the capacitor, and the charge flowing to the capacitor per cycle is always higher than in the case of the PV-TENG; the stored charge is increased 1.55-fold compared with the PV-TENG after just 25 cycles. Similar to the electric quantity increase, the energy output of the CV-TENG under a capacitance load is also obviously elevated. The energy flowing to the capacitor per cycle for the CV-TENG is boosted to 6.15 mJ at its maximum, which is over 3 times that of the PV-TENG, exhibiting the unique benefits of the CV-TENG in terms of energy output (Fig. 3e).

Furthermore, there is strong correlation between the energy flowing to the capacitor per cycle and the voltage of the capacitor; the energy output per cycle increases as the voltage of the capacitor increases until it achieves the maximum average power and then decreases (Fig. 3f). Therefore, just as it is necessary to find the matched resistance of a TENG under a resistance load to obtain the maximum average power output, it is also important to find the matched capacitor voltage for a TENG under a capacitance load to obtain the maximum average power output. The instantaneous power (P_{ins}^C), instantaneous energy (E_{ins}^C), and average power (P_{AP}^C) of a capacitor can be represented using the following equations:

$$P_{ins}^C = U_C i = C U_C \frac{dU_C}{dt} \quad (2)$$

$$E_{ins}^C = \int_0^T P_{ins}^C dt = \int_0^T C U_C \frac{dU_C}{dt} dt = 0.5 C U_C^2 \quad (3)$$

$$P_{AP}^C = \frac{E_{ins}^C}{T} = \frac{C U_C^2}{2T} \quad (4)$$

where C is the capacitance of the capacitor, U_C represents the voltage of the capacitor, and T is the charging time. In addition to the relationship between the energy stored in the capacitor and time exhibited in Fig. 3g and h, another relationship can be presented between the average power output of the TENG under a capacitance load and the required point-in-time (that is, the time when the capacitor needs to be discharged). As shown in Fig. 3g, the PV-TENG obtains a maximum average power output of 2.33 mW when the voltage is 436 V. The CV-TENG acquires a maximum average power output of 4.56 mW when the voltage is 887 V, which is a 1.96-fold increase over the PV-TENG (Fig. 3h). The maximum average power outputs of the PV-TENG and CV-TENG can be obtained sustainably upon power management at their respective matched voltages (Fig. 3i).

Moreover, the maximum average power values of the CV-TENG and PV-TENG under a capacitance load at different frequencies are also exhibited in Fig. 3j, k and Fig. S11 (ESI[†]). The CV-TENG

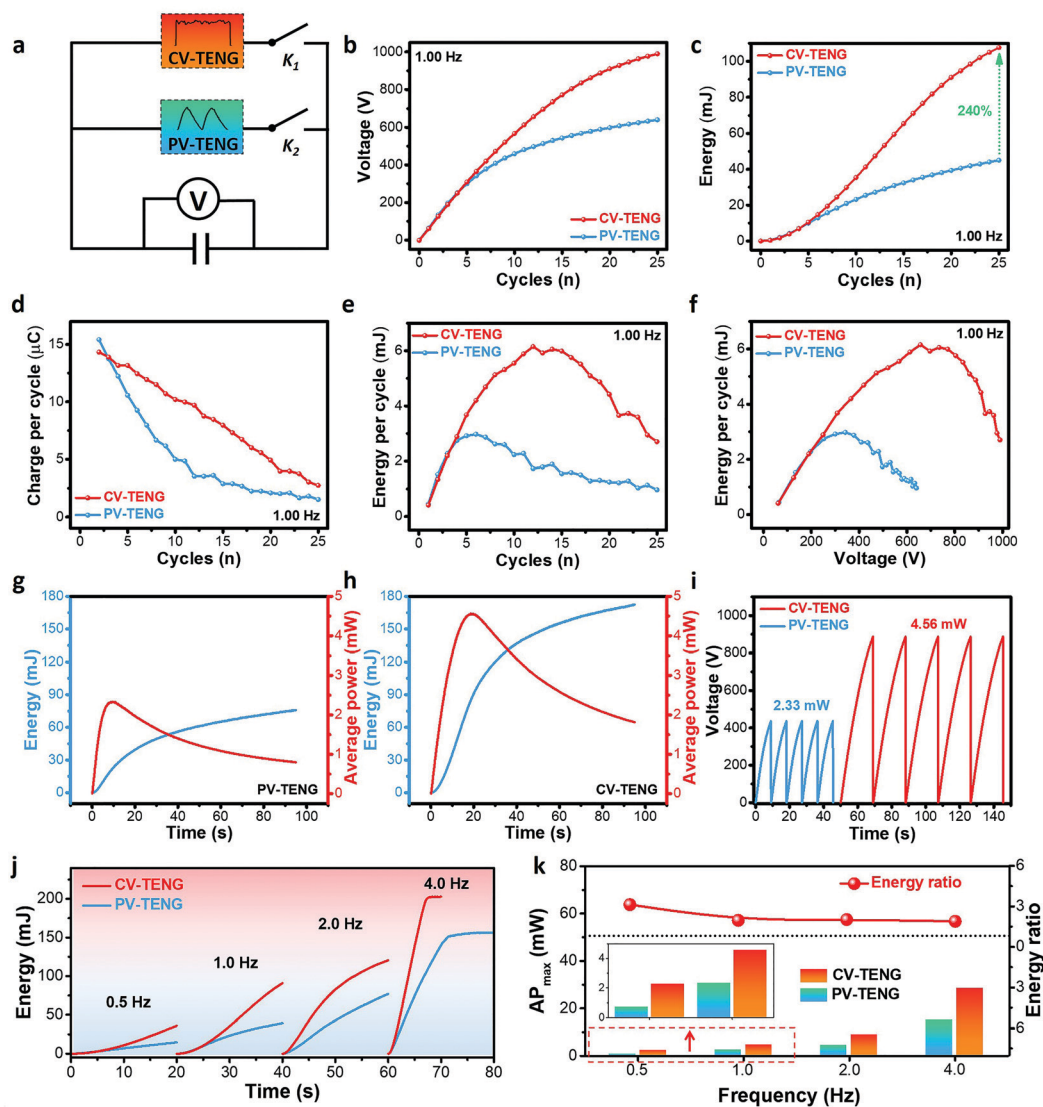


Fig. 3 The output performance of a CV-TENG under a capacitance load. (a) The circuit connections between the two types of TENG and a capacitor. (b) The charging voltage of the capacitor, (c) the stored energy of the capacitor, (d) the amount of charge flowing to the capacitor per cycle, and (e) the energy flowing to the capacitor per cycle as a function of the cycle number when charged by the CV-TENG and the PV-TENG. (f) The energy flowing to the capacitor per cycle versus the voltage of the capacitor when charged by the CV-TENG and PV-TENG. The stored energy and average power changes over time when charged by the (g) PV-TENG and (h) CV-TENG. (i) Power management to obtain the maximum average power from the CV-TENG and PV-TENG. (j) The stored energy of the capacitor over time when charged by the CV-TENG and PV-TENG at different frequencies. (k) The maximum average power (AP) of the CV-TENG and PV-TENG under a capacitance load and their energy ratios at different frequencies.

obtains maximum average power values of 2.28, 4.56, 8.75, and 28.34 mW at 0.5, 1, 2, and 4 Hz, respectively, while the PV-TENG only acquires maximum average power values of 0.73, 2.32, 4.34, and 14.97 mW, respectively. The CV-TENG can obtain higher average power levels than the PV-TENG at all different frequencies under a capacitance load. It even shows a 3-fold increase compared with the PV-TENG in response to low-frequency mechanical energy input (0.5 Hz), exhibiting unique advantages in terms of harvesting low-frequency mechanical energy efficiently.

The dynamic process of charge transfer under a capacitance load

The energy output under a resistance load can be used to explore the maximum energy output of a TENG, and the energy

output under a capacitance load can be used to help find an appropriate power management method to obtain the maximum energy output. To explore why the CV-TENG has the ability to enhance the electric quantity and energy output compared with the PV-TENG, an insight into the dynamic process of charge transfer under a capacitance load is proposed based on the electrical principles of TENGs (Fig. 4). As shown in Fig. 4a, modelling the dynamic process of a TENG charging a capacitor should focus on the real-time performance of the dynamic process during every cycle, which will overcome the limitations of early models which only discussed the transferred charge rather than pulsed voltage effects.³⁶ During the dynamic process, it is necessary to measure the real-time values

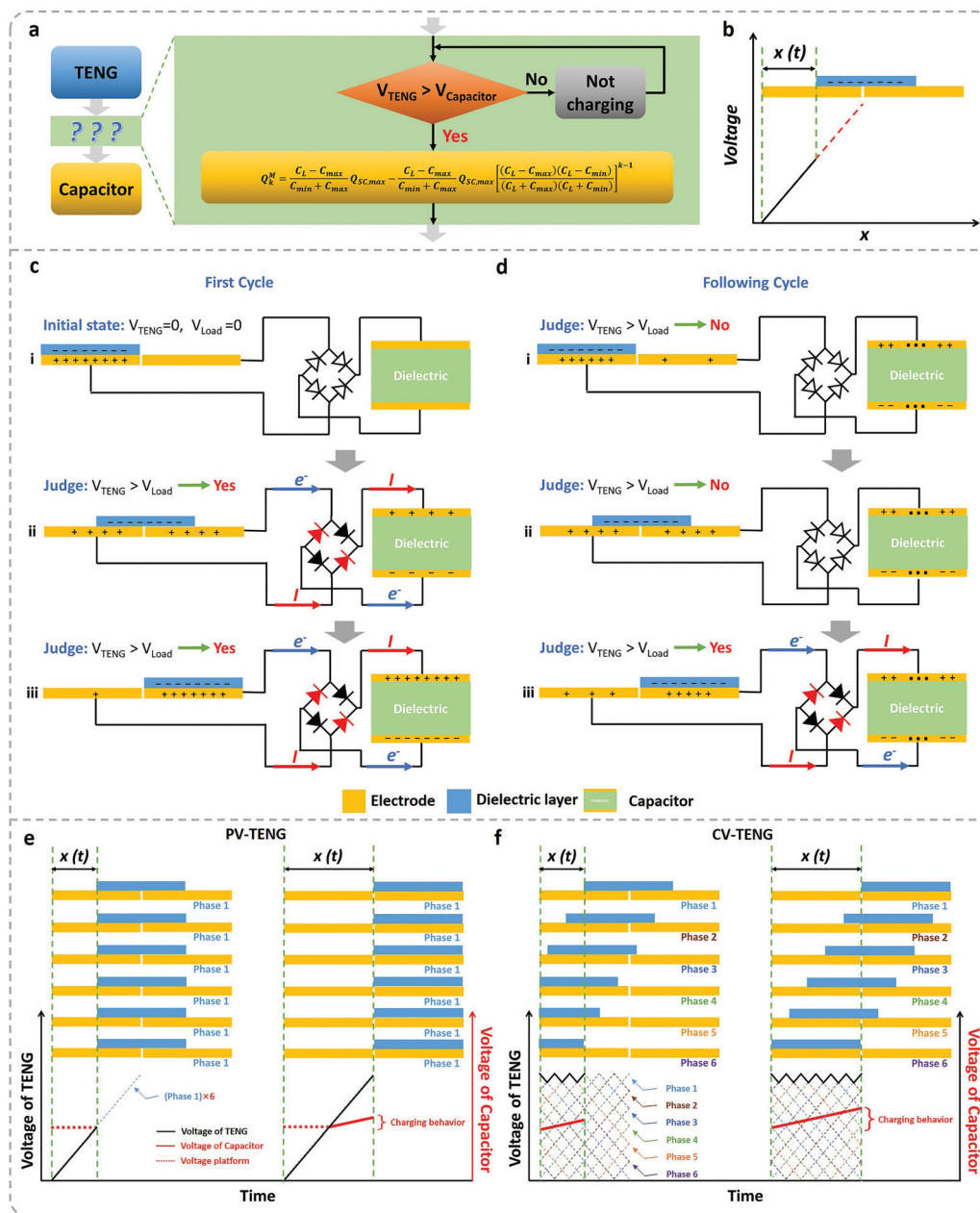


Fig. 4 The dynamic process of charge transfer under a capacitance load. (a) A dynamic behavior diagram of a TENG charging a capacitor. (b) The change in the TENG voltage versus the motion path in free-standing mode. Logic representations of (c) the first cycle and (d) subsequent cycles for a TENG charging a capacitor. Schematic illustrations of the charging principles of the (e) PV-TENG and (f) CV-TENG under a capacitance load.

of the TENG voltage and capacitor voltage. Only when the real-time TENG voltage is greater than the capacitor voltage, will charging behavior occur. Generally, it generates the same amount of electric quantity in every cycle under short-circuit conditions or under a resistance load due to coupling effects involving contact electrification and electrostatic induction, while this behavior changes when the TENG starts to charge the capacitor. The charge generated due to contact electrification and electrostatic induction during the process of a TENG charging a capacitor can be divided into two types: transferred charge (TC) and reserved charge (RC), where TC is used to

charge the capacitor and RC plays a crucial role in maintaining the same voltage between the TENG and the capacitor. The electric quantity (Q_k^M) of TC can be derived as follows:³⁵

$$Q_k^M = \frac{C_L - C_{\text{max}}}{C_{\text{min}} + C_{\text{max}}} Q_{\text{SC,max}} - \frac{C_L - C_{\text{max}}}{C_{\text{min}} + C_{\text{max}}} Q_{\text{SC,max}} \left[\frac{(C_L - C_{\text{max}})(C_L - C_{\text{min}})}{(C_L + C_{\text{max}})(C_L + C_{\text{min}})} \right]^{k-1} \quad (5)$$

where Q_k^M is the charge on node M at the time of the k th cycle, M is a node on the circuit of the TENG charging the capacitor, C_L

is the capacitance of the capacitor, and C_{\max} and C_{\min} are the maximum and minimum values of the variable capacitance of the TENG. Detailed information is provided in Fig. S12 and Note S3 (ESI[†]). The proportion of TC decreases as the voltage of the capacitor increases, which is consistent with the experimental data shown in Fig. 3d. It is useful to note that the above dynamic process is applicable to all categories of TENGs because TENG category information is not utilized in this dynamic process.

Taking free-standing mode as an example, a simple model to describe the relationship between the TENG voltage and the motion path is fabricated in Fig. 4b. There is strong correlation between the voltage of the open-circuit TENG and the motion path.³⁷ Detailed information relating to the relationship between the TENG voltage and the motion path is exhibited in Fig. S13 and Note S4 (ESI[†]). A model with a TENG charging a capacitor with a rectifier is shown in Fig. 4c and d, exhibiting the relationship between the charging behavior and the motion path in every cycle. In the first cycle, there is a quasi-charging state in which the voltages of both the TENG and the capacitor are zero, as shown in state i in Fig. 4c. When the TENG starts moving, charging behavior occurs and continues until the voltage of the TENG reaches its maximum (state ii in Fig. 4c and state iii in Fig. 4c). In subsequent cycles, charging behavior does not occur in state i in Fig. 4d, because the voltage of the TENG is lower than the voltage of the capacitor. When the TENG starts moving, it is necessary to judge whether the voltage of the TENG is higher than that of the capacitor, as shown in state ii in Fig. 4d. If the answer is no, then charging behavior does not take place. If the answer is yes, then charging behavior occurs until state iii in Fig. 4d is reached.

Meanwhile, two integrated models are fabricated to describe the differences between the PV-TENG and CV-TENG based on six individual TENGs presenting the same and different phases, respectively, as shown in Fig. 4e and f. Detailed circuit connections are shown in Fig. S14 (ESI[†]). The PV-TENG model retains the same pulsed voltage shape as a single TENG unit (Fig. 4e). It has a lower energy output due to the voltage platform of the capacitor sustaining for a longer time during one cycle as the charging cycle number increases, particularly under conditions in which the capacitor is at high voltage. However, the CV-TENG model possesses six different phases, and it has the ability to transform pulse-voltage output into constant-voltage output based on the linear circuit superposition principle (Fig. 4f). Therefore, the CV-TENG is endowed with the feature of charging the capacitor all the time, greatly increasing the energy output and improving the charging efficiency of the TENG.

Demonstrations of CV-TENG application.

Due to its excellent constant-current/voltage performance, the CV-TENG can be regarded as an individual power source that can convert environmental energy into electrical energy, suited to driving various commercial electronics (Fig. 5a). Moreover, the phase-shift design can be applied to any rotational or even sliding motion, including wind- and water-driven motion,

owing to the ease of manufacturability. For simple and direct comparison, a CV-TENG could light 132 LEDs without flickering, while a PV-TENG could light 132 LEDs with flickering under the same mechanical input (Fig. 5b, c and Movie S1 ESI[†]). It is obvious that the brightness of LEDs powered by the CV-TENG is higher than those powered by the PV-TENG due to the superiority of the CV-TENG in terms of electric quantity output, even though the same mechanical input is provided (Fig. 2c). Moreover, four white lights (rated power: 9×4 W) can also be lit by the CV-TENG, providing sufficient illumination for reading printed text in complete darkness (Fig. 5d and Movie S2 ESI[†]). Meanwhile, the CV-TENG could sustain 4 multifunctional digital hygrothermographs under continuous operation, as demonstrated in Fig. 5e and Movie S3 (ESI[†]).

Although it is a huge leap to use a CV-TENG to directly drive electronics without energy storage, a major challenge still exists because the energy transfer efficiency is very low when powering electronic devices because the high voltage and low current characteristics of TENGs do not match existing electronics.¹⁷ Recently, the power management of PV-TENGs has attracted more attention, which is desirable when using TENGs to power electronics and is of great significance for promoting the commercialization of TENGs in the near future.^{5,18,31} Therefore, a power management method for the CV-TENG is urgently needed to help match it to ordinary electronics efficiently (Fig. 5f). In reality, regardless of whether a CV-TENG or PV-TENG is used, the idea of power management is the same, that is, converting high-voltage energy into a high current.^{5,18,31} Therefore, a universal power management strategy for TENGs can be summarized in two steps, as shown in Fig. 5g. A temporary capacitor stores energy from the TENG when switch K_1 is closed and then the stored energy is released to a power management system when switch K_2 is closed. The TENG can provide continuous energy output by this process being repeated. Due to the charging behavior being unsustainable in the second half cycle when using a PV-TENG, previous research has focused on type-I power management, in which the temporary capacitor tends to be discharged to zero to obtain the maximum average power output from the PV-TENG in the first half cycle, as shown in Fig. 5h and Fig. S15 (ESI[†]).^{5,18,31} The energy-output efficiency of the PV-TENG can be represented as follows:

$$\eta = \frac{E_C}{E} = \frac{\int_0^t C U_C \frac{dU_C}{dt} dt}{U C U_C} = 0.5 \left(1 - e^{-t/RC} \right) \quad (6)$$

where E_C is the stored energy of the capacitor, E represents the total electrical energy of the TENG, U is the voltage of the TENG, C is the capacitance load of the capacitor, U_C is the voltage of the capacitor, R is the inherent resistance of the TENG, and t is the charging time; detailed calculations are shown in Note S5 (ESI[†]). From eqn (6), the energy-output efficiency is very low in the initial stage of charging because the voltage of the capacitor is low and the energy output does not increase much. Even though the energy-output efficiency is gradually elevated as time goes by, the maximum energy-output efficiency is only

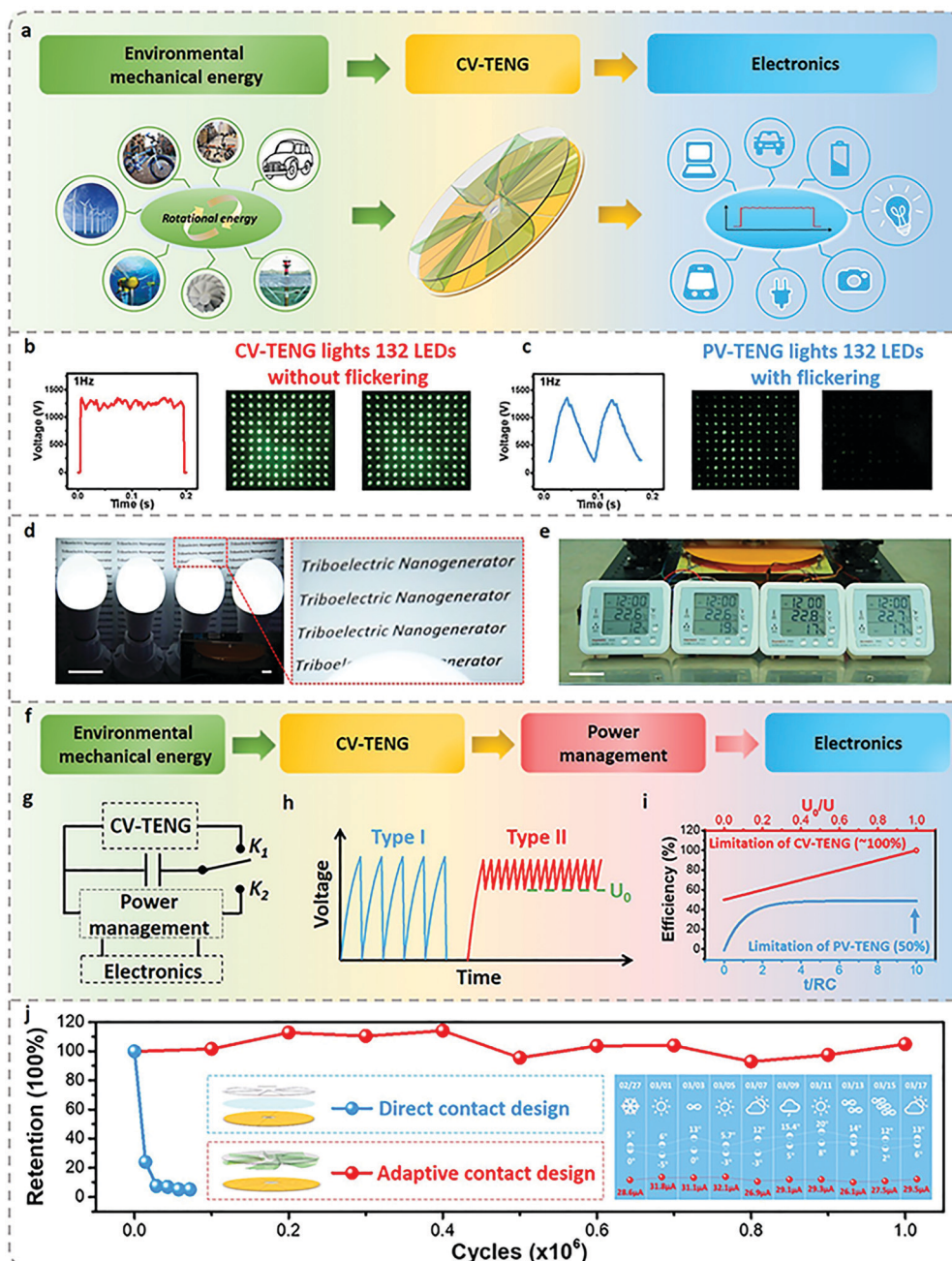


Fig. 5 Demonstrations of the application of the CV-TENG. (a) A schematic illustration of a CV-TENG driving electronics directly. (b) A photograph of 132 LEDs directly powered by a CV-TENG without flickering at a rotation frequency of 1 Hz. (c) A photograph of 132 LEDs directly powered by a PV-TENG with flickering at a rotation frequency of 1 Hz. (d) A photograph of 4 white lights that are directly powered by a CV-TENG in complete darkness at a rotation frequency of 4 Hz (scale bar: 5 cm); inset: a zoomed-in view of the setup. (e) A photograph of 4 hygrometers directly powered by a CV-TENG at a rotation frequency of 4 Hz; scale bar: 5 cm. (f) A schematic illustration of highly efficient CV-TENG use via power management. (g) Universal circuit connections for obtaining a highly efficient CV-TENG. (h) Two methods of power management for the CV-TENG (Type I: discharging to zero; Type II: discharging to U_0). (i) Changes in energy-output efficiency versus U_0/U and t/RC . (j) The long-term durability of the TENG in adaptive contact design and direct contact design set-ups; inset: the average current from a CV-TENG with adaptable contact design on different days under 1 Hz during durability testing.

50% (Fig. 5i), which coincides with previous reports based on $V-Q$ plots.¹⁵

However, the temporary capacitor could also be discharged to a non-zero value (U_0) using type-II power management to obtain maximum average power output from the CV-TENG, as

shown in Fig. 5j and Fig. S15 (ESI[†]). The energy-output efficiency can be calculated as follows:

$$\eta = \frac{\Delta E_C}{\Delta E} = \frac{0.5(U + U_0) - Ue^{-t/RC} + 0.5(U - U_0)e^{-2t/RC}}{U(1 - e^{-t/RC})} \quad (7)$$

It is clear that the energy-output efficiency varies with time t and is related to U and U_0 . Detailed calculations are given in Note S5 (ESI[†]). The energy-output efficiency can be further simplified when the charging behavior achieves equilibrium as follows:

$$\eta = \lim \frac{\Delta E_C}{\Delta E} = \frac{0.5(U + U_0)}{U} \quad (8)$$

Obviously, the above energy-output efficiency is greater than 50% as the voltage U_0 increases. Type-II power management greatly promotes the energy output and efficiency close to 100% can even be acquired when U_0 is close to U , overcoming the limitation of the maximum energy-output efficiency of the PV-TENG being only up to 50% (Fig. 5i).¹⁵ However, this boost of the average power when using type-II power management is not very efficient in the case of a PV-TENG since a pulse-voltage set-up has poor abilities to ensure sustainable charging behavior. Different from a PV-TENG, which needs to depend on a matching capacitor to obtain maximum average power, the constant-voltage characteristics give a CV-TENG more operational space for power management; it is no longer confined to the best matching capacitance and inductance, but it can be chosen appropriately according to the need of the application. This breakthrough provides more diverse ways to reduce the obstacles preventing the commercialization of TENGs.

In experiments under a resistance load and capacitance load and based on theoretical calculations relating to power management, it has been shown that the CV-TENG has a higher energy output and better efficiency than the PV-TENG, providing a paradigm for new types of TENGs and power management designs. Furthermore, the dynamic process of charge transfer under a capacitance load gives a theoretical guide to improving the energy-output efficiency of TENGs toward 100%. A specific way to improve performance could be through the addition of a high-frequency mechanical switch linked with the mechanical motion. This ensures that the temporary capacitor has been charged before the voltage of the temporary capacitor happens to drop, always keeping within a high voltage range with small fluctuations, followed by cycling. Detailed measurements need to be optimized in conjunction with the entire circuit, placing high importance on the design of the switch. It is also necessary to choose more suitable electronic components to use the energy of the CV-TENG efficiently to match existing electronics in the near future.

In addition to its excellent energy-output efficiency, the CV-TENG also shows a long service lifetime due to the introduction of adaptive contact design between the dielectric layer and electrode during the TENG manufacturing process (Fig. 5j). Compared with direct contact design, adaptive contact design not only leads to excellent robustness, but it also makes the TENG practically reliable and durable. It exhibits stable output for 1 000 000 cycles without obvious performance attenuation, showing excellent stability when using the TENG as a competent distributed power source (the average current values of the CV-TENG on different days at 1 Hz during durability testing are shown in the inset of Fig. 5j). Meanwhile, the relationship

between the gap distance and the electrical output of the TENG is presented in Fig. S17 (ESI[†]), which gives a guide to obtaining higher electrical output.

Conclusions

In this work, a CV-TENG is realized *via* a phase-shift design, based on a PV-TENG, and it produces a significantly higher energy output than a PV-TENG for driving conventional electronics directly. It outputs constant current with a crest factor of 1.03, and its average power under a resistance load is increased 1.9-fold compared with a conventional PV-TENG without a phase-shift design. The average power is even increased over 3-fold compared with a PV-TENG under a capacitance load at a frequency of 0.5 Hz, which exhibits the superiority of the CV-TENG when harvesting low-frequency mechanical energy. Meanwhile, we also gain insight into the dynamic process of charge transfer under a capacitance load, providing insight for improving the energy-output efficiency of CV-TENGs toward 100%, theoretically higher than the PV-TENG limit of only 50%. Furthermore, the lifetime of the CV-TENG is tremendously extended as a result of using an adaptive contact design between the electrode and dielectric material. Given its exceptional energy output and extremely simple structure, the phase-shift design presented in this work provides a universal and practical approach for transforming a conventional pulse-voltage output into a constant-voltage output, promoting the energy-output efficiency of TENGs; this can provide a paradigm shift when it comes to achieving high-efficiency TENGs, and there are widespread application prospects in the field of distributed energy.

Moreover, this is the first time that a quantitative comparison between CV-TENGs and PV-TENGs has been carried out from the aspect of the charge transfer process. As a result, similar to how it is necessary to find the matched resistance for a TENG under a resistance load to obtain the maximum average power output, it is also significant to find the matched capacitor voltage for a TENG under a capacitance load to obtain the maximum average power output. Therefore, this work provides a general method to harvest the maximum average power output of a TENG under a capacitance load, playing a crucial role in the further development of power management and self-charging power systems. Our study also indicates an effective power management idea for obtaining maximum TENG energy-output efficiency, which can also be applied to other kinds of CV-TENGs, *e.g.*, DC-TENGs based on coupling effects involving contact electrification and electrostatic breakdown. Future work will involve the optimization of power management to further achieve high energy-transfer efficiency and energy-storage efficiency over an entire circuit system.

Excellent TENG output performance is an essential prerequisite when a TENG acts as a distributed power source or a key component of a self-powered system. Previous research has widely investigated aspects such as materials, structure, the medium environment, and auxiliary circuits to enhance

triboelectric charge density and improve the energy output from PV-TENGs. As shown here, the phase-shift design could not only utilize the manufacturing process used for conventional PV-TENGs, but it could also improve the energy output further; it provides a universal and practical approach for acquiring constant-current/voltage output. Furthermore, the paradigm used to enhance the average power of TENGs in this work can be applied to TENG networks, which are generally used to harvest water-wave energy. Due to the disordered features of wave energy, there are naturally different phases in TENG networks. Therefore, this work points to an effective approach for moving the average power close to the peak power when using TENGs for large-scale wave-energy harvesting.

Materials and methods

Fabrication of the triboelectric nanogenerator

Rotor: (1) a disc-shaped acrylic sheet was cut out as a substrate with a radius of 15 cm and thickness of 3 mm using a laser cutter; (2) radially arrayed trenches were created, which define the location of the dielectric layer on the substrate, using laser cutting; (3) the dielectric layer was pasted in the trenches; (4) through-holes were drilled at the center of the substrate for mounting it to a mechanical stage using screws. **Stator:** (1) a disc-shaped sheet was cut out as a substrate with a radius of 15 cm; (2) a layer of Cu (1.6 mm) was plated as electrodes using PCB technology; (3) every pair of electrodes was connected to a rectifier and the pairs were connected in parallel.

Experimental setup for electric measurements

(1) A rotary motor was mounted in inverted fashion on a working stage; (2) the shaft was inserted into the motor and into the central hole of the rotor; (3) the rotor and the stator were aligned with coaxial alignment; (4) the height was adjusted so that the dielectric layer on the rotor and the stator were in contact.

Electrical measurements

A programmable electrometer (Keithley model-6514) was adopted to test the current output of the TENG under a resistance load. A mixed domain oscilloscope (MDO3024; the attenuation coefficient of the high voltage probe is 1000 and the circuit input impedance is 100 M Ω) was used to test the open-circuit voltage of the TENG. An electrostatic voltmeter (Trek Model-347) was used to obtain voltage curves from the capacitor.

Author contributions

X. L. and J. W. conceived the idea. X. L., C. Z., and Y. G. designed the experiments and performed data measurements. X. L. and Y. G. analyzed the data. Z. Z., Y. H., O. Y., L. L., and L. Z. helped with the experiments. X. L., Z. Z., L. L., and J. W. drafted the manuscript. X. L., J. W. and Z. L. W. supervised this work. All authors discussed the results and commented on the manuscript.

Conflicts of interest

The authors declare no competing financial interests.

Acknowledgements

The authors acknowledge financial support from the National Key R & D Project from the Minister of Science and Technology (2021YFA1201602), the National Natural Science Foundation of China (No. 61774016, 21773009, U21A20147, and 22109013), the China Postdoctoral Science Foundation (2021M703171), the Fundamental Research Funds for the Central Universities (E1E46802), and the Beijing Municipal Science & Technology Commission (Z171100000317001, Z171100002017017, and Y3993113DF). The authors also thank Kai Yin and Qi Zhang for their help with using some software for this work.

References

- 1 S. Chu and A. Majumdar, *Nature*, 2012, **488**, 294.
- 2 H. Boudet, *Nat. Energy*, 2019, **4**, 446.
- 3 X. Zhao, H. Askari and J. Chen, *Joule*, 2021, **5**, 1391.
- 4 R. Jain, J. Qin and R. Rajagopal, *Nat. Energy*, 2017, **2**, 17112.
- 5 Z. Wang, W. Liu, W. He, H. Guo, L. Long, Y. Xi, X. Wang, A. Liu and C. Hu, *Joule*, 2021, **5**, 441.
- 6 C. Chen, Z. Wen, J. Shi, X. Jian, P. Li, J. Yeow and X. Sun, *Nat. Commun.*, 2020, **11**, 4143.
- 7 Z. L. Wang, *Adv. Energy Mater.*, 2020, **10**, 2000137.
- 8 S. Cui, L. Zhou, D. Liu, S. Li, L. Liu, S. Chen, Z. Zhao, W. Yuan, Z. L. Wang and J. Wang, *Matter*, 2022, **5**, 1–14.
- 9 C. Zhang, L. He, L. Zhou, O. Yang, W. Yuan, X. Wei, B. Liu, L. Lu, J. Wang and Z. L. Wang, *Joule*, 2021, **5**, 1613–1623.
- 10 J. Jiang, Q. Guan, Y. Liu, X. Sun and Z. Wen, *Adv. Funct. Mater.*, 2021, **31**, 2105380.
- 11 Z. L. Wang, *Rep. Prog. Phys.*, 2021, **84**, 096505.
- 12 X. Wang, J. Song, J. Liu and Z. L. Wang, *Science*, 2007, **316**, 102–105.
- 13 X. Yin, D. Liu, L. Zhou, X. Li, C. Zhang, P. Cheng, H. Guo, W. Song, J. Wang and Z. L. Wang, *ACS Nano*, 2019, **13**, 698–705.
- 14 H. Wang, L. Xu, Y. Bai and Z. L. Wang, *Nat. Commun.*, 2020, **11**, 4203.
- 15 Y. Zi, J. Wang, S. Wang, S. Li, Z. Wen, H. Guo and Z. L. Wang, *Nat. Commun.*, 2016, **7**, 10987.
- 16 Y. Zi, S. Niu, J. Wang, Z. Wen, W. Tang and Z. L. Wang, *Nat. Commun.*, 2015, **6**, 8376.
- 17 X. Cheng, W. Tang, Y. Song, H. Chen, H. Zhang and Z. L. Wang, *Nano Energy*, 2019, **61**, 517–532.
- 18 H. Wu, S. Wang, Z. Wang and Y. Zi, *Nat. Commun.*, 2021, **12**, 5470.
- 19 H. Ryu, J. Lee, U. Khan, S. Kwak, R. Hinchet and S. Kim, *Energy Environ. Sci.*, 2018, **11**, 2057–2063.
- 20 G. Zhu, J. Chen, T. Zhang, Q. Jing and Z. L. Wang, *Nat. Commun.*, 2013, **5**, 3426.
- 21 Z. Zhao, L. Zhou, S. Li, D. Liu, Y. Li, Y. Gao, Y. Liu, Y. Dai, J. Wang and Z. L. Wang, *Nat. Commun.*, 2021, **12**, 4686.

- 22 J. Liang, Z. Zhang, Q. Xue, Y. Zheng, X. Wu, Y. Huang, X. Wang, C. Qin, Z. Chen and C. Chen, *Energy Environ. Sci.*, 2021, **10**, 1039.
- 23 X. Xu, L. Xiao, Y. Jia, Z. Wu, F. Wang, Y. Wang, N. Haugen and H. Huang, *Energy Environ. Sci.*, 2018, **11**, 2198–2207.
- 24 Y. Hong, L. Jin, B. Wang, J. Liao, B. He, T. Yang, Z. Long, P. Li, Z. Zhang, S. Liu, Y. Lee, B. Khoo and Z. Yang, *Energy Environ. Sci.*, 2021, **14**, 6574–6585.
- 25 Y. Hu, X. Li, Z. Zhao, C. Zhang, L. Zhou, Y. Li, Y. Liu, J. Wang and Z. L. Wang, *Small methods*, 2021, **10**, 2100936.
- 26 X. Li, X. Yin, Z. Zhao, L. Zhou, D. Liu, C. Zhang, C. Zhang, W. Zhang, S. Li, J. Wang and Z. L. Wang, *Adv. Energy Mater.*, 2020, **10**, 1903024.
- 27 P. Chen, J. An, R. Cheng, S. Shu, A. Berbille, T. Jiang and Z. L. Wang, *Energy Environ. Sci.*, 2021, **14**, 4523–4532.
- 28 J. Wang, Y. Li, Z. Xie, Y. Xu, J. Zhou, T. Cheng, H. Zhao and Z. L. Wang, *Adv. Energy Mater.*, 2020, **10**, 1904227.
- 29 R. Dharmasena, H. Cronin, R. Dorey and S. Silva, *Nano Energy*, 2020, **75**, 104887.
- 30 Z. Wu, S. Wang, Z. Cao, R. Ding and X. Ye, *Nano Energy*, 2021, **83**, 105787.
- 31 Z. Wang, Q. Tang, C. Shan, Y. Du, W. He, S. Fu, G. Li, A. Liu, W. Liu and C. Hu, *Energy Environ. Sci.*, 2021, **14**, 6627.
- 32 S. Niu, S. Wang, L. Lin, Y. Liu, Y. Zhou, Y. Hu and Z. L. Wang, *Energy Environ. Sci.*, 2013, **6**, 3576.
- 33 X. Li, X. Yin, W. Wang, H. Zhao, D. Liu, L. Zhou, C. Zhang and J. Wang, *Nano Energy*, 2019, **56**, 792–798.
- 34 J. Luo and Z. L. Wang, *Energy Storage Mater.*, 2019, **23**, 617–628.
- 35 H. Lei, Y. Chen, Z. Gao, Z. Wen and X. Sun, *J. Mater. Chem. A*, 2021, **9**, 20100.
- 36 S. Niu, Y. Liu, Y. Zhou, S. Wang, L. Lin and Z. L. Wang, *IEEE T. Electron. Dev.*, 2015, **62**, 641–647.
- 37 S. Niu, Y. Liu, X. Chen, S. Wang, Y. Zhou, L. Lin, Y. Xie and Z. L. Wang, *Nano Energy*, 2015, **12**, 760–774.